Inorganic Chemistry

Article

pubs.acs.org/IC

Synthesis and Properties of Type-I Clathrate Phases $Rb_{8-x-t}K_x\square_tAu_yGe_{46-y}$

H. Zhang,*[†,‡] M. Baitinger,[†] L. Fang,[†,§] W. Schnelle,[†] H. Borrmann,[†] U. Burkhardt,[†] A. Ormeci,[†] J. T. Zhao,[‡] and Yu. Grin[†]

[†]Max-Planck-Institut für Chemische Physik fester Stoffe, Nöthnitzer Straße 40, 01187 Dresden, Germany

[‡]Key Laboratory of Transparent Opto-Functional Inorganic Materials, Shanghai Institute of Ceramics, Chinese Academy of Sciences, 1295 Dingxi Road, Shanghai 200050, China

[§]Key Laboratory of Nonferrous Materials and New Processing Technology, Ministry of Education, Guilin University of Technology, 12 Jiangan Road, Qixing, Guilin, Guangxi, China

ABSTRACT: Type-I clathrates $Rb_{8-x-t}K_x\square_tAu_yGe_{46-y}$ are synthesized from Rb_4Ge_9, K_4Ge_9, Au, and Ge. Crystal structures and compositions are determined by single-crystal and powder X-ray diffraction methods. The lattice parameters are 10.8103(2), 10.7956(2), 10.7850(2), and 10.7723(2) Å in space group $Pm\bar{3}n$ for $Rb_{7.88(2)}Au_{2.47(2)}Ge_{43.53(2)}$, $Rb_{3.69(4)}K_{4.31(4)}Au_{2.17(2)}Ge_{43.83(2)}$, $Rb_{1.66(5)}K_{6.34(5)}Au_{2.17(1)}Ge_{43.83(1)}$, and $K_{6.71(4)}Au_{2.28(2)}Ge_{43.72(2)}$, respectively. Bonding analysis for $Rb_8Au_6Ge_{40}$ suggests ionic interaction of Rb with the framework besides covalent interactions between Ge and Au/Ge. $Rb_{7.88}Au_{2.47}Ge_{43.53}$ and $K_{6.71(4)}Au_{2.28}Ge_{43.72}$ are both diamagnetic. The heat capacity of $K_{6.71}Au_{2.28}Ge_{43.72}$ is analyzed. Transport properties of $Rb_{7.88}Au_{2.47}Ge_{43.53}$ reveal *n*-type conducting, and low thermal conductivity.

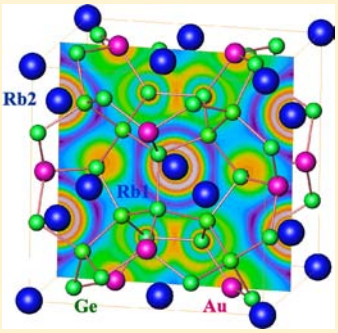

INTRODUCTION

Clathrate compounds comprise host frameworks that embrace guest species in polyhedral cages.[1−6] Inorganic clathrates form some structure types according to respective polyhedral types and their arrangements, such as type-I clathrates $K_7B_7Si_{39}$,[7] $Ge_{38}P_8I_8$,[8] $Ge_{46-x}I_xI_8$,[9] and $K_{8-x}Si_{46}$,[10,11] type-II clathrates $Cs_8Na_{16}Si_{136}$[12] and $\square_{24}Ge_{136}$ ($\square$ denotes a vacant cationic position[2]), type-III clathrate $Si_{172-x}P_xTe_y$,[13] type-VIII clathrates α-$Eu_8Ga_{16}Ge_{30}$[14] and α-$Ba_8Ga_{16}Sn_{30}$,[15] type-IX clathrate K_8Sn_{25},[16] type-X clathrates $Ge_{79}P_{29}S_{18}Te_6$,[17] etc. Clathrates may be classified into cationic, anionic, and neutral according to the charge distribution between the framework and guest atoms: e.g., anionic clathrates $K_7B_7Si_{39}$, K_7Si_{46}, $Cs_8Na_{16}Si_{136}$, α-$Eu_8Ga_{16}Ge_{30}$, and $K_{7.4}Sn_{25}$; cationic clathrates $Ge_{38}P_8I_8$, $Si_{172-x}P_xTe_y$, and $Ge_{79}P_{29}S_{18}Te_6$, and neutral clathrate $\square_{24}Ge_{136}$, as well as water clathrates or clathrate hydrates.[18]

For the synthesis of type-I A_8E_{46} and type-II $A_{24-x}E_{136}$ (A = Na, K, Rb, Cs; E = Si, Ge) clathrates, thermal decomposition of A_4E_4 phases under dynamic vacuum was used.[9,19] Recently, high yields of crystalline $A_{8-x}Si_{46}$ (A = Na, K) are achieved by the oxidation of A_4Si_4 with gaseous HCl or H_2O.[10] The guest-free type-II clathrate $\square_{24}Ge_{136}$ is synthesized by the reaction of $Na_{12}Ge_{17}$ with an ionic liquid (DTAC/$AlCl_3$) at 300 °C.[2] The Hg-substituted type-I clathrates $A_8Hg_{3+x}Ge_{43-x}$ are synthesized from binary precursors A_4Ge_9 (A = K, Rb) with Hg and Ge.[20] $K_7B_7Si_{39}$[7] is obtained directly by the heating of K, B, and Si elements.

The recent impetuous interest in clathrates of tetrels (elements of group 14), in which the host framework is based on Si, Ge, or Sn atoms, is motivated in particular by the search for a new generation of efficient thermoelectric materials. High thermoelectric figures of merit ($ZT > 1$) are realized in Ga-substituted germanium clathrates $Ba_8Ga_{16}Ge_{30}$[21] and $Sr_8Ga_{16}Ge_{30}$.[22] High ZT is discovered also for Au-substituted germanium clathrate $Ba_8Au_xGe_{46-x-y}\square_y$,[23−25] with the highest value of 0.9 for $Ba_8Au_{5.3}Ge_{40.7}$.[26] The Zintl−Klemm rule offers a simple explanation for the formation of electronically balanced clathrates with partial substitutions on the framework and guest atom sites.[21,22,26] Herein the synthesis and properties of Au-substituted clathrate phases of alkali metals $Rb_{8-x-t}K_x\square_tAu_yGe_{46-y}$ are reported.

EXPERIMENTAL SECTION

Synthesis. The target compositions $Rb_{8-x}K_xAu_{2.7}Ge_{43.3}$ are chosen according the Zintl−Klemm rule in order to obtain charge-balanced systems according to $(Rb_{8-x}K_x)^+Au^{3-}{}_{2.7}Ge^0{}_{43.3}$. Hereafter, starting compositions will be used in the text for the samples' identification. The refined compositions will be used in the Results and Discussion section.

Precursors Rb_4Ge_9 and K_4Ge_9 are obtained by heating Rb or K and Ge at 650 °C for 24 h in tantalum crucibles. Subsequently, Rb_4Ge_9, K_4Ge_9, Au, and Ge are loaded into Ta containers in molar ratio Rb_4Ge_9:K_4Ge_9:Au:Ge = (8−x) : x : 10.8 : 101.2 (x = 0, 4, 6, 8). The containers are welded in an argon-filled glovebox [$c(O_2)$ and $c(H_2O)$ ≤ 1 ppm] and sealed in a quartz ampule under vacuum. After 2 weeks of heating at 700 °C, gray products are obtained and washed with distilled water and acetone.

Received: November 7, 2012
Published: August 14, 2013

   dx.doi.org/10.1021/ic3024315 | *Inorg. Chem.* 2013, 52, 9720−9726

Composition. The appropriately prepared metallographic specimens of $Rb_8Au_{2.7}Ge_{43.3}$ are investigated on a Philips XL 30 scanning electron microscope equipped with a LaB_6 cathode. The chemical composition is established with energy-dispersive X-ray spectroscopy (EDXS; EDAX Genesis Software V 4.61) using a Si (Li) detector attached at the scanning electron microscope. Compositions are calculated from the background-corrected intensities of the X-ray lines K *K*, Rb *L*, Au *L*, and Ge *K*, which were excited by the electron beam at a 25 kV acceleration voltage. A standardless method with ZAF-matrix corrections is used.

Powder X-ray Diffraction (XRD). The samples are characterized by Guinier technique (Huber Image Plate Camera G670; Cu $K\alpha_1$ radiation; λ = 1.54056 Å; 3.0° < 2θ < 100.3°; step width 0.005°), using LaB_6 (a = 4.15693 Å) as the internal standard. The lattice parameters are refined by means of a least-squares technique with the program package *WinCSD*.[27]

Single-crystal XRD. A small single crystal is seperated from the block polycrystalline specimen $Rb_8Au_{2.7}Ge_{43.3}$ is fixed on the top of a glass capillary with epoxy. Diffraction data are collected with a four-circle diffraction system (Rigaku AFC-7; Saturn 724 detector; Mo $K\alpha$ radiation; λ = 0.71073 Å). Absorption correction is performed with a multiscan procedure. The crystal structure refinement is performed by a full-matrix least-squares procedure within the *WinCSD* program package.[27] For crystal structure presentation, the program *Diamond 3.0* is used.[28]

Physical Properties. Magnetization of $Rb_{7.88}Au_{2.47}Ge_{43.53}$ and $K_{6.71}Au_{2.28}Ge_{43.72}$ was measured from 1.8 to 400 K in a SQUID magnetometer (MPMS, Quantum Design). The heat capacity of $K_{6.71}Au_{2.28}Ge_{43.72}$ as well as the thermal and electrical transport properties of $Rb_{7.88}Au_{2.47}Ge_{43.53}$ were determined applying the PPMS (Quantum Design, HC or TT option, respectively).

Calculation Procedures. Calculation of the electronic structure and analysis of the chemical bonding are carried out for the ordered model with the composition $Rb_8Au_6Ge_{40}$ (with the 6*c* site occupied completely by Au). The model adopts the lattice parameter and atomic positions from the single-crystal X-ray refinement of $Rb_{7.80}Au_{1.92}Ge_{44.08}$ reported in this study (Tables 1 and 2). The *TB–LMTO–ASA* program package is used.[29] The von Barth–Hedin exchange potential[30] is employed for the local density approximation (LDA) calculations. The radial scalar-relativistic Dirac equation is solved to obtain the partial waves. Because the calculation within the atomic sphere approximation (ASA) includes corrections for the neglect of interstitial regions and partial waves of higher order,[31] an addition of empty spheres is not necessary. The following radii of the atomic spheres are applied for the calculations: r(Rb1) = 2.480 Å, r(Rb2) = 2.692 Å, r(Au1) = 1.491 Å, r(Ge2) = 1.374 Å, and r(Ge3) = 1.382 Å. For calculation, a basis set of orbitals containing Rb(5*s*), Au(6*s*,6*p*,5*d*), and Ge(4*s*,4*p*) is employed for a self-consistent calculation, with Rb(5*p*,4*d*,4*f*), Au(5*f*), and Ge(3*d*) functions being downfolded.

For a better description of the electronic density within the large cavities of the crystal structure, additional calculations are performed using a full-potential all-electron local orbital code *FPLO*[32] within the LDA. Relativistic effects are incorporated on a scalar-relativistic level.

The electron localizability indicator (ELI, γ) was evaluated in the ELI-D representation according to refs 33–35 with an ELI-D module within the program package *TB–LMTO–ASA*.[29] Topological analysis of the electron density, i.e., estimation of the shapes, volumes, and charges of the atoms following the quantum theory of atoms in molecules (QTAIM[36]), and of the ELI, e.g., localization of the ELI maxima as fingerprints of the direct covalent atomic interactions, is performed with the program *DGrid*.[37]

RESULTS AND DISCUSSION

The crystal structure of $Rb_{7.80}Au_{1.92}Ge_{44.08}$ is determined by direct methods[27] that allow the localization of all atomic positions. During the initial steps of the refinement, all framework atoms are treated as Ge, while the guest atoms are set as Rb in the space group $Pm\bar{3}n$. The subsequent refinement shows that the isotropic atomic displacement parameters (ADPs) for the Ge1 atoms (6*c*) are notably smaller than those for other Ge atoms. This indicates a partial Au substitution at this site. Location of the transition metals at this position is a common feature for the intermetallic clathrates with a low amount of substitution. Special care is taken to uncover the reason for the relatively high ADPs for Rb1 (2*a*) and Rb2 (6*d*). Refinement of the occupancy factors reveals a slightly reduced occupation for both positions. In addition, the positions of the Rb2 atoms are better described as shifted from the symmetry center at ($^1/_4$, 0, $^1/_2$). These assumptions yield similar displacement parameters for both Rb sites.

Table 1. Data Collection and Structure Parameters for $Rb_{7.80}Au_{1.92}Ge_{44.08}$

composition	$Rb_{7.80(12)}Au_{1.92(6)}Ge_{44.08(6)}$
a (Å)	10.8203(3)
formula mass (g fu^{-1})	4246.8
cell volume (Å^3)	1266.8(1)
F(000) (electrons)	1851.1
no. of atoms in a cell	53.8
calcd density (g cm^{-3})	5.5619(5)
abs coeff (cm^{-1})	386.62
radiation and wavelength (Å)	Mo $K\alpha$, 0.71073
mode of refinement	$F(hkl)$
restriction	$F(hkl) > 2\sigma(F)$
maximal 2θ (deg) and sin θ/λ (Å^{-1})	67.8, 0.78
no. of measured reflns	6455
no. of reflns with $F > 2\sigma(F)$	5847
R_{eq}, R_F	0.058, 0.051

Because of disorder in the crystal structure, all reflections with $I > 2\sigma(I)$ were used for refinement. The estimated standard deviations for refined parameters were recalculated according to the number of symmetry-equivalent reflections. The refinement converges at $R(F)$ = 0.051 with 24 parameters. Further details of data collection and structure refinement details are given in Table 1, final atomic coordinates and displacement parameters are shown in Table 2, and the shortest distances are collected in Table 3.

The atomic arrangement of $Rb_{7.80}Au_{1.92}Ge_{44.08}$ is characteristic for a type-I clathrate structure (Figure 1). It features a cage network of four-bonded atoms forming two types of cages: 20-vertex pentagonal dodecahedra (Rb1 in the cages with partial occupancy) and 24-vertex hexakaidecahedra (split Rb2 in the cages with partial occupancy) in the ratio 2:6 resulting in eight cavities per unit cell. Au1 atoms share the hexagon-ring sites (6*c*) with Ge1. Other sites are occupied by Ge2 at 16*i* and Ge3 at 24*k*. In contrast to the recently studied $Ba_8Ni_{3.5}Ge_{42.1}\square_{0.4}$[38], the isotropic displacement of the Ge3 position shows that no defects are present at the 6*c* site, and the difference in the effective size of the Au and Ge atoms is small [compared to the notable difference between metallic radii of r(Au) = 1.442 Å and r(Ge) = 1.225 Å, the difference between the covalent radii of r_{cov}(Au) = 1.34 Å and r_{cov}(Ge) = 1.225 Å is smaller].[44]

The composition $Rb_{7.80(12)}Au_{1.92(6)}Ge_{44.08(6)}$ established from the crystal structure refinement deviates from the composition of the bulk sample, from which the single crystal is separated, and from the target electron-balanced composition according to the Zintl count. This may be caused by chemical non-homogeneity and nonequilibrium of the reaction products obtained at relatively low temperature. In contrast to the equilibrium single-crystal growth of electron-balanced $Ba_8Au_{5.3}Ge_{40.7}$,[26] the prepartion conditions used in the present

dx.doi.org/10.1021/ic3024315 | *Inorg. Chem.* 2013, 52, 9720–9726

Table 2. Atomic Coordinates and Equivalent Isotropic (B_{eq}) and Anisotropic (B_{ij}) Displacement Parameters (Å^2) for $Rb_{7.80}Au_{1.92}Ge_{44.08}$

atom	site	x	y	z	occupancy	B_{eq}[a]
Rb1	2*a*	0	0	0	0.95(1)	1.36(3)
Rb2	24*k*	0.2444(4)	0.0160(2)	$^1/_2$	0.246(2)	1.28(8)
Au1/Ge1	6*c*	0	$^1/_4$	$^1/_2$	0.321(4)/0.679	1.11(2)
Ge2	16*i*	0.18392(3)	*x*	*x*	1	1.011(7)
Ge3	24*k*	0.11884(5)	0.30784(5)	0	1	1.07(1)

atom	B_{11}	B_{22}	B_{33}	B_{12}	B_{13}	B_{23}
Rb1	1.36(4)	B_{11}	B_{11}	0	0	0
Rb2	1.33(4)	1.1(2)	1.47(13)	0.17(8)	0	0
Ge1/Au1	0.96(2)	1.40(3)	0.96(2)	0	0	0
Ge2	1.01(1)	B_{11}	B_{11}	−0.031(9)	B_{12}	B_{12}
Ge3	1.04(2)	1.15(2)	1.01(2)	−0.03(1)	0	0

[a] $B_{eq} = 4/3[B_{11}(a^*)^2a^2 + B_{22}(b^*)^2b^2 + B_{33}(c^*)^2c^2 + 2B_{12}(a^*)(b^*)\ ab\ \cos\gamma + 2B_{13}(a^*)(c^*)\ ac\ \cos\beta + 2B_{23}(b^*)(c^*)\ bc\ \cos\alpha]$.

Table 3. Shortest Interatomic Distances (Å) for $Rb_{7.80}Au_{1.92}Ge_{44.08}$

Rb1−8Ge2	3.4469(4)	Rb2−1Ge3	3.991(2)
Rb1−12Ge3	3.5706(6)	Rb2−2Ge2	4.100(1)
Rb2−2Ge3	3.543(3)	Rb2−2Ge2	4.181(2)
Rb2−2Ge3	3.596(3)	Rb2−2Ge3	4.1845(9)
Rb2−1Au1/Ge1	3.661(3)	Rb2−1Ge3	4.335(2)
Rb2−2Ge3	3.667(3)	Au1/Ge1−4Ge3	2.5173(6)
Rb2−2Ge3	3.792(3)	Ge2−1Ge2	2.4768(5)
Rb2−2Au1/Ge1	3.872(3)	Ge2−3Ge3	2.5008(5)
Rb2−2Ge2	3.886(2)	Ge3−2Ge2	2.5008(5)
Rb2−1Au1/Ge1	3.909(3)	Ge3−1Au/Ge1	2.5173(6)
Rb2−2Ge2	3.927(1)	Ge3−1Ge3	2.5720(8)

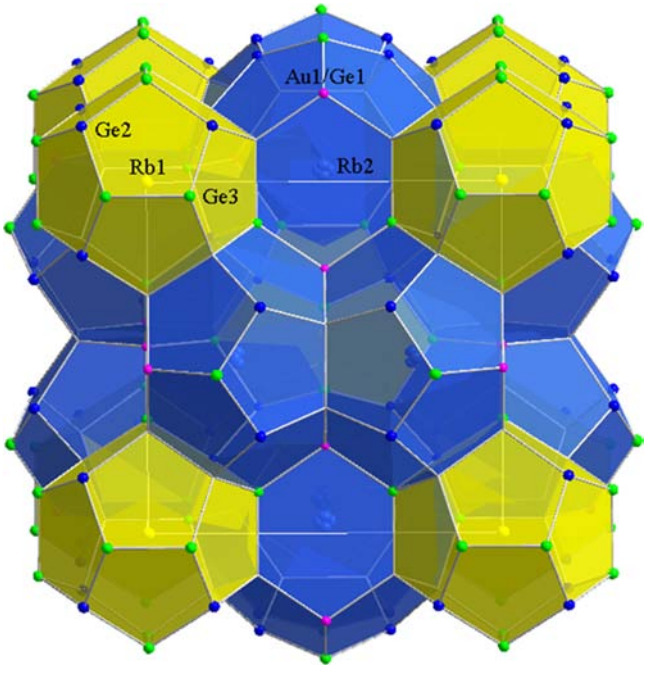

Figure 1. Crystal structure of $Rb_{7.80}Au_{1.92}Ge_{44.08}$: yellow, Rb1 at the 2*a* site; blue, Rb2 at the 24*k* site with 24.6% occupancy; pink, Au1/Ge1 at the 6*c* site; blue, Ge2 at the 16*i* site; green, Ge3 at the 24*k* site.

work yield chemical compositions that clearly deviate from the Zintl count.

The composition of the bulk part of the sample $Rb_{7.88}Au_{2.47}Ge_{43.53}$ is investigated by the EDXS technique. The surface morphology of the sample is shown in Figure 2. The composition established from three different areas on the surface varies quite strongly because of the dependence of the results on the tilt angle of the surface area used for analysis.

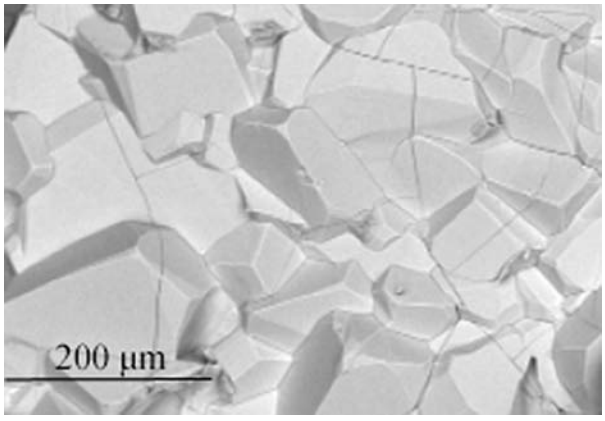

Figure 2. Surface morphology of $Rb_{7.88}Au_{2.47}Ge_{43.53}$. The composition is established at three different areas by EDXS.

The compositions and site occupancies of samples $Rb_{7.88}Au_{2.47}Ge_{43.53}$, $Rb_{3.69}K_{4.31}Au_{2.17}Ge_{43.83}$, $Rb_{1.66}K_{6.34}Au_{2.17}Ge_{43.83}$, and $K_{6.71}Au_{2.28}Ge_{43.72}$ are further studied by refinement of the crystal structures using the *WinCSD* package.[27] The XRD patterns along with the theoretical and difference profiles are shown in Figure 3. All reflections are indexed in space group $Pm\bar{3}n$ except some residual peaks found in $Rb_{7.88}Au_{2.47}Ge_{43.53}$. The results are given in Table 4. For comparison, the data for Rb_8Ge_{44} and K_8Ge_{44} are presented.[39,40] Fractional atomic coordinates, site occupancies, and isotropic ADPs are collected in Table 5.

Ge-by-Au substitution within the framework influences the lattice parameter more efficiently than Rb-by-K substitution in the cages. While the implementation of Au atoms in the framework (per unit cell) increases the lattice parameter up to 0.1 Å, complete alkali-metal exchange results only in half of this change. In the framework cavities, the K atoms first replace the Rb atoms in the small cages and subsequently in the large cages (Figure 4). Analysis of the site occupancy parameters reveals higher Au content in the polycrystalline $Rb_{7.88}Au_{2.47}Ge_{43.53}$ compared with single-crystal data. The observed composition is very close to the Zintl count, which may cause the bad-metal-like or semiconductor-like behavior in the electronic and

dx.doi.org/10.1021/ic3024315 | *Inorg. Chem.* 2013, 52, 9720−9726

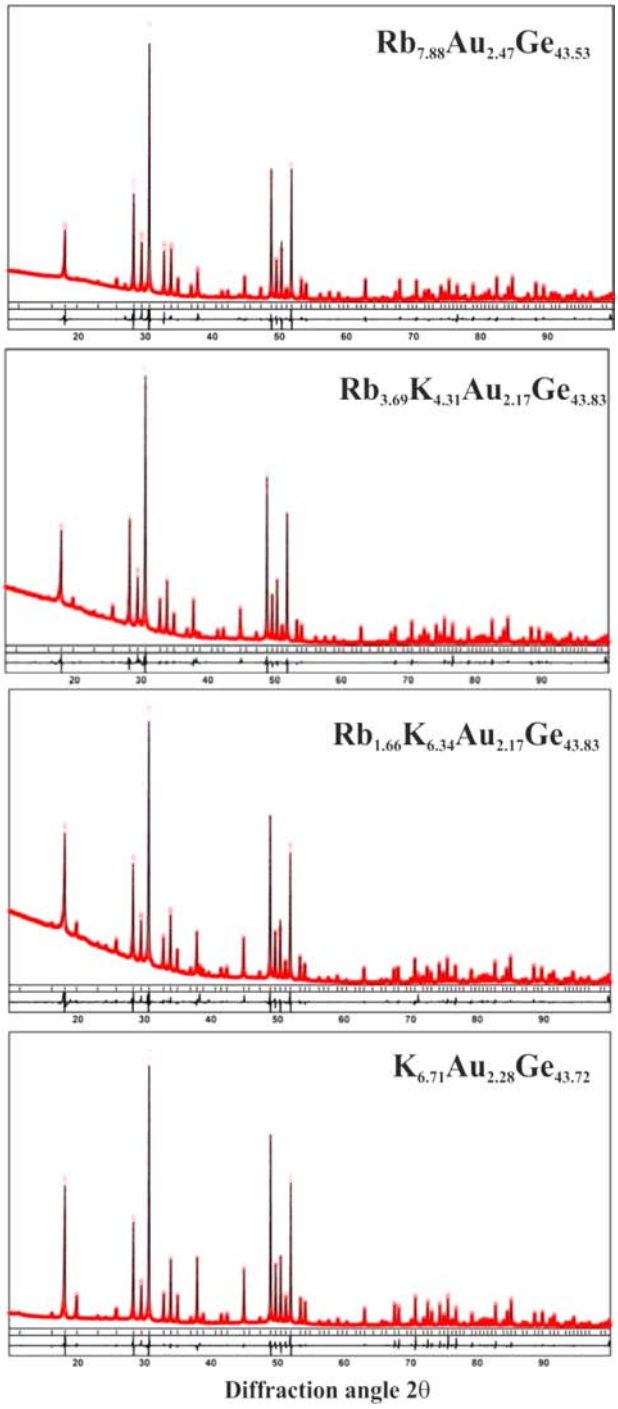

Figure 3. Powder XRD patterns (Cu $K\alpha_1$ radiation) of $Rb_{7.88}Au_{2.47}Ge_{43.53}$, $Rb_{3.69}K_{4.31}Au_{2.17}Ge_{43.83}$, $Rb_{1.66}K_{6.34}Au_{2.17}Ge_{43.83}$, and $K_{6.71}Au_{2.28}Ge_{43.72}$: (red) experimental data points; (black) calculated intensities. Tick marks correspond to the calculated positions of the Bragg reflections. The difference between the observed and theoretical patterns is shown in the bottom part.

thermal transport properties. In order to prove this assumption, calculation of the band structure and analysis of the chemical bonding are performed.

The ordered model of $Rb_8Au_6Ge_{40}$ is the closest to the experimentally found composition within the experimental unit cell and space group with the 6*c* position occupied by Au atoms and 16*i* and 24*k* sites filled with Ge atoms. The electronic density of states (DOS) reveals a distribution expected from the Zintl count $[Rb^+]_8[Au^{3-}]_6[Ge^0]_{40}\cdot 10p^+$, namely, a gap above the Fermi level with bonding states partially nonoccupied (Figure 5, LMTO calculation). Similarly to $Ba_8Au_6Ge_{40}$, the whole electronic DOS is formed mainly by the *s* and *p* states of Ge and the *d* states of Au. The s states of Rb and Au are present in a wide range of energies below the Fermi level and overlap with the *s* and *p* states of Ge as well as the *d* states of Au. Such a distribution of DOS is in agreement with the picture of an ionic guest−host interaction in intermetallic clathrates. Assuming the rigid-band behavior by a reduction of the Au content, the Fermi level would achieve the upper border of the bonding region at $y = 2.65$, being well in accordance with the expected value of $y = 2.67$ from the Zintl count above under the conditions of the charge balance.

For an understanding of thermal transport in clathrates, the interaction between the cations in the cavities and the framework atoms is the key issue. For Ba-containing clathrates, the direct interaction between the Ba and Au atoms is suggested to play an important role in reduction of the lattice thermal conductivity.[21,22,26] In order to shed light on atomic interactions, a combined analysis of the electron density and ELI is performed.

Well in agreement with the common understanding of the chemical bonding in clathrates, the QTAIM basins reveal charge transfer of the electrons from Rb to the framework (effective charges of +0.69 for Rb1 and +0.77 for Rb2; FPLO result). Within the framework, the charge distribution follows the electronegativity of the elements. Au, the most electronegative element, concentrates the most charge (−0.86), whereas the Ge species remain mainly neutral (−0.08 for Ge2 and +0.02 for Ge3).

The ELI in $Rb_8Au_6Ge_{40}$ shows a spherical distribution in the inner shells of all atoms (Figure 6), indicating that the electrons of these shells do not contribute markedly to the interactions within the valence region. The maxima of ELI-D are found between the atoms of the network, revealing covalent (polar) interactions between the Ge and Au atoms. In contrast to $Ba_8Au_6Ge_{40}$, no dedicated maxima of ELI-D were observed on the Rb−Au contacts, suggesting the only ionic interaction of Rb with the framework. This finding is confirmed in thermal transport (see below).

The magnetic susceptibility $\chi = M/H$ versus temperature of $Rb_{7.88}Au_{2.47}Ge_{43.53}$ and $K_{6.71}Au_{2.28}Ge_{43.72}$ reveals a diamagnetic behavior of both compounds. The extrapolated susceptibilities are -1.4×10^{-3} and -1.1×10^{-3} emu mol^{-1} for $Rb_{7.88}Au_{2.47}Ge_{43.53}$ and $K_{6.71}Au_{2.28}Ge_{43.72}$, respectively. The Rb compounf is stronger diamagnetic than the K ones, as is expected from the larger closed-electron-shell contribution of Rb.

The specific heat capacity $C_p(T)$ of $K_{6.71}Au_{2.28}Ge_{43.72}$ is presented in Figure 7. For clathrates and similar compounds, it may be described by the sum of three contributions: the electronic contribution $C_e = \gamma T$ and the lattice contributions c_l from both the rigid cage-forming network and the guest atoms within the cages. In a simplistic approach, the latter two contributions may be described by a Debye term and an Einstein term, respectively (see, e.g., ref 41). The existence of a low-energy Einstein contribution is often motivated by the presence of a maximum in the representation $C_l/T^3 = (C_p - \gamma T)/T^3$, which basically illustrates deviations from the Debye T^3 law valid in the low-T limit. The inset in Figure 7 demonstrates that also for $K_{6.71}Au_{2.28}Ge_{43.72}$ such a maximum is observed. However, it is well-known that quite a number of elements and

dx.doi.org/10.1021/ic3024315 | *Inorg. Chem.* 2013, 52, 9720−9726

Table 4. Lattice Parameters and Compositions of $Rb_{8-x-t}K_x\square_tAu_yGe_{46-y}$

starting composition	lattice parameter (Å)	refined composition	residuals R_I, R_P
Rb_8Ge_{44}[39]	10.70	Rb_8Ge_{44}	
$Rb_8Au_{2.7}Ge_{43.3}$	10.8103(2)	$Rb_{7.88(2)}Au_{2.47(2)}Ge_{43.53(2)}$	5.71, 13.79
$Rb_4K_4Au_{2.7}Ge_{43.3}$	10.7956(2)	$Rb_{3.69(4)}K_{4.31(4)}Au_{2.17(2)}Ge_{43.83(2)}$	5.27, 11.12
$Rb_2K_6Au_{2.7}Ge_{43.3}$	10.7850(2)	$Rb_{1.66(5)}K_{6.34(5)}Au_{2.17(1)}Ge_{43.83(1)}$	5.47, 14.55
$K_8Au_{2.7}Ge_{43.3}$	10.7723(2)	$K_{6.71(4)}Au_{2.28(2)}Ge_{43.72(2)}$	5.16, 11.64
K_8Ge_{44}[40]	10.686(4)	K_8Ge_{44}	

Table 5. Atomic Coordinates, Site Occupancies, and Isotropic ADPs (Å^2) for $Rb_{7.88}Au_{2.47}Ge_{43.53}$, $Rb_{3.69}K_{4.31}Au_{2.17}Ge_{43.83}$, $Rb_{1.66}K_{6.34}Au_{2.17}Ge_{43.83}$, and $K_{6.71}Au_{2.28}Ge_{43.72}$

atom	site	x	y	z	occupancy	B_{iso}
			$Rb_{7.88}Au_{2.47}Ge_{43.53}$			
Rb1	2*a*	0	0	0	0.940(9)	0.66(6)
Rb2	6*d*	$^1/_4$	$^1/_2$	0	1	2.15(4)
Au1/Ge1	6*c*	$^1/_4$	0	$^1/_2$	0.411(3)/0.589	1.16(3)
Ge2	16*i*	0.18445(7)	*x*	*x*	1	0.96(2)
Ge3	24*k*	0	0.30695(9)	0.11885(9)	1	0.47(3)
			$Rb_{3.69}K_{4.31}Au_{2.17}Ge_{43.83}$			
Rb1/K1	2*a*	0	0	0	0.13(2)/0.87	0.37(2)
Rb2/K2	6*d*	$^1/_4$	$^1/_2$	0	0.572(7)/0.428	2.29(5)
Au1/Ge1	6*c*	$^1/_4$	0	$^1/_2$	0.362(4)/0.638	0.74(2)
Ge2	16*i*	0.18341(6)	*x*	*x*	1	0.82(1)
Ge3	24*k*	0	0.30855(7)	0.11857(7)	1	0.54(2)
			$Rb_{1.66}K_{6.34}Au_{2.17}Ge_{43.83}$			
Rb1/K1	2*a*	0	0	0	0.15(2)/0.85	1.25(11)
Rb2/K2	6*d*	$^1/_4$	$^1/_2$	0	0.228(8)/0.772	1.96(8)
Au1/Ge1	6*c*	$^1/_4$	0	$^1/_2$	0.361(2)/0.639	0.57(3)
Ge2	16*i*	0.18377(7)	*x*	*x*	1	0.66(1)
Ge3	24*k*	0	0.30860(9)	0.11851(9)	1	0.50(3)
			$K_{6.71}Au_{2.28}Ge_{43.72}$			
K1	2*a*	0	0	0	1	1.17(7)
K2	6*d*	$^1/_4$	$^1/_2$	0	0.784(6)	1.82(10)
Au1/Ge1	6*c*	$^1/_4$	0	$^1/_2$	0.381(3)/0.619	1.25(3)
Ge2	16*i*	0.18378(6)	*x*	*x*	1	1.22(1)
Ge3	24*k*	0	0.30836(8)	0.11805(7)	1	0.87(3)

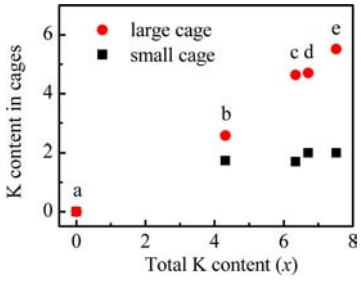

Figure 4. K content in the small and large cages versus the total K content in $Rb_{7.88}Au_{2.47}Ge_{43.53}$ (a), $Rb_{3.69}K_{4.31}Au_{2.17}Ge_{43.83}$ (b), $Rb_{1.66}K_{6.34}Au_{2.17}Ge_{43.83}$ (c), $K_{6.71}Au_{2.28}Ge_{43.72}$ (d), and K_8Ge_{44} (e).[40]

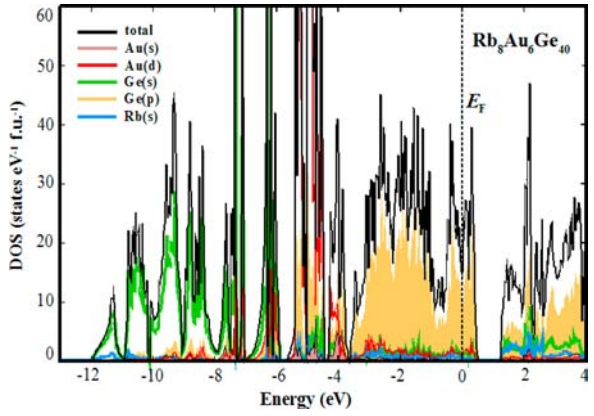

Figure 5. Calculated total electronic DOS and selected atomic contributions for $Rb_8Au_6Ge_{40}$.

compounds having simple structures (like the diamond type) show a maximum in such a C_l/T^3 plot (for an extensive discussion, see, e.g., ref 42).

Corresponding combined fits[43] to the data of the present compound (temperature ranges up to 10 or 14 K) result in a good description (Figure 7, main panel). However, the fits did not lead to a realistic spectral weight for the Einstein term; thus, no clear low-lying localized phonon mode could be identified, as was the case for high-quality single crystals of $Na_{24}Si_{136}$.[42] This observation might be due to a relatively large structural inhomogeneity in the present material.

Resorting to the standard description of specific heat at low temperatures, the data can be expressed as $C_p = \gamma T + \beta T^3$. The resulting parameters for $K_{6.71}Au_{2.28}Ge_{43.72}$ (from a fit of the data with $T < 3.1$ K) are $\gamma = 15.0$ mJ mol^{-1} K^{-2} and $\beta = 4.60$ mJ

dx.doi.org/10.1021/ic3024315 | Inorg. Chem. 2013, 52, 9720−9726

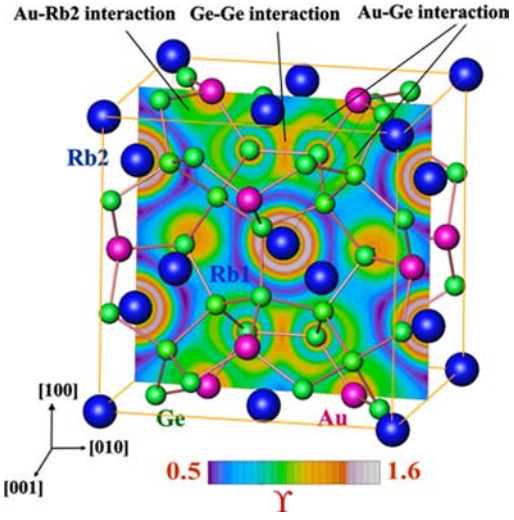

Figure 6. Distribution of the ELI in the plane at z = 0.5 in $Rb_8Au_6Ge_{40}$.

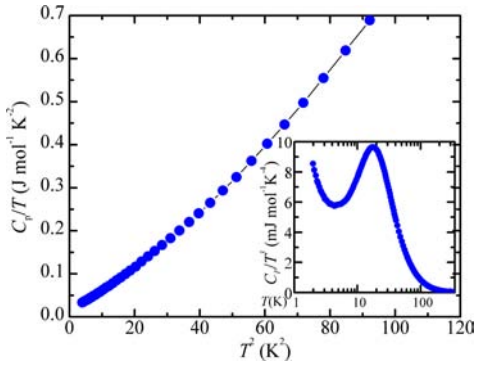

Figure 7. Heat capacity of $K_{6.71}Au_{2.28}Ge_{43.72}$ plotted as $C_p/T(T^2)$. Inset: low-temperature part as C_l/T^3 vs temperature.

mol^{-1} K^{-4}. The resulting Debye temperature Θ_D of ≈280 K is well comparable to that of $Ba_8Au_{5.3}Ge_{40.7}$ (Θ_D ≈ 270 K[26]). Using the free-electron model, an electronic DOS of ≈6.4 states eV^{-1} fu^{-1} at the Fermi level may be estimated for $K_{6.71}Au_{2.28}Ge_{43.72}$.

The temperature dependences of the electrical resistivity ρ, the Seebeck coefficient α of the thermoelectric power, the thermal conductivity κ, and the dimensionless thermoelectric figure of merit ZT for $Rb_{7.88}Au_{2.47}Ge_{43.53}$ are given in Figure 8. The compound shows a high electrical resistivity, which decreases with temperature, indicating a thermally activated conduction mechanism in this temperature range. The negative Seebeck coefficient suggests that the majority of charge carriers are electrons. Both findings are well in agreement with the composition obtained from the crystal structure determination, $[Rb^+]_{7.80}[Au^{3-}]_{1.92}[Ge^0]_{44.08}\cdot 2.04e^-$, and even in the better with one determined on the bulk material $[Rb^+]_{7.88}[Au^{3-}]_{2.47}[Ge^0]_{44.08}\cdot 0.47e^-$. The thermal conductivity is low and increases with the temperature. The absence of a local maximum indicates the typical "phonon-glass behavior" of filled clathrates. An estimate by the Wiedemann-Franz rule results in a very small electronic contribution to $\kappa(T)$. Thus, because of the low charge-carrier concentration, the total thermal conductivity reflects mainly the lattice behavior. The thermal conductivity of $Rb_{7.88}Au_{2.47}Ge_{43.53}$ is generally higher than that found for $Ba_8Au_{5.3}Ge_{40.7}$,[26] being well in agreement with analysis of the chemical bonding (no direct Rb−Au interaction). The thermoelectric figure of merit ZT for $Rb_{7.88}Au_{2.47}Ge_{43.53}$ is very low even at 350 K. The obtained value is diminishingly low compared with that of SPS-sintered $Ba_8Au_{5.3}Ge_{40.7}$, which reaches ZT = 0.92 at 600 K.[26]

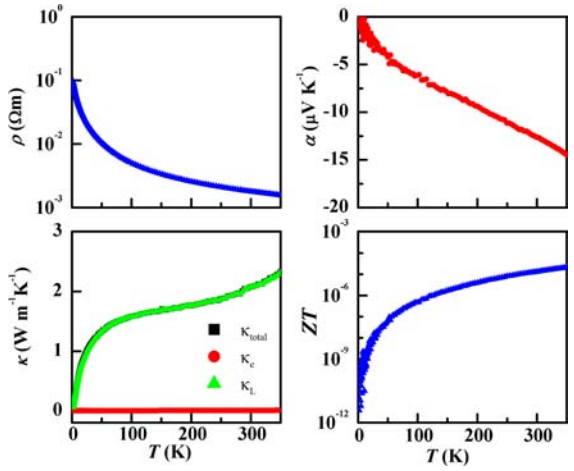

Figure 8. Temperature dependences of the electrical conductivity ρ, Seebeck coefficient α, thermal conductivity κ [total conductivity κ_{total} and its electronic (κ_e) and lattice (κ_L) contributions], and thermoelectric figure of merit ZT for $Rb_{7.88}Au_{2.47}Ge_{43.53}$.

CONCLUSIONS

The solid solution $Rb_{8-x-t}K_x\square_tAu_yGe_{46-y}$ crystallizes in the type-I clathrate structure. Analysis of the electronic structure and chemical bonding reveals charge transfer from the alkali metals to the framework (ionic interaction) and covalent (polar) bonding within the framework. Contrary to the known barium representative $Ba_8Au_{5.3}Ge_{40.7}$, no direct Rb−Au interaction was found in rubidium clathrate. The compounds $Rb_{7.88}Au_{2.47}Ge_{43.53}$ and $K_{6.71}Au_{2.28}Ge_{43.72}$ are diamagnetic. $Rb_{7.88}Au_{2.47}Ge_{43.53}$ shows n-type charge carriers and thermally activated conduction below 350 K, albeit with a low Seebeck coefficient. Its thermal conductivity is dominated by the lattice contribution, in agreement with analysis of the chemical bonding.

AUTHOR INFORMATION

Corresponding Author

*E-mail: huizhangmpg@hotmail.com.

Notes

The authors declare no competing financial interest.

ACKNOWLEDGMENTS

This work was supported by the Innovation Group for the MST (Grant 50821004), Partner Group MPG/CAS at SICCAS, and CAS/SAFEA International Partnership Program for Creative Research Teams. This work was also supported by Natural Science Foundation of China (No. 21261007, 21061004).

REFERENCES

(1) Kasper, J. S.; Hagenmuller, P.; Pouchard, M.; Cros, C. *Science* **1965**, *150*, 1713−1714.

(2) Guloy, A. M.; Ramlau, R.; Tang, Z.; Schnelle, W.; Baitinger, M.; Grin, Yu. *Nature* **2006**, *443*, 320−323.

dx.doi.org/10.1021/ic3024315 | *Inorg. Chem.* 2013, 52, 9720−9726

(3) Gryko, J.; McMillan, P. F.; Marzke, R. F.; Ramachandran, G. K.; Patton, D.; Deb, S. K.; Sankey, O. F. *Phys. Rev. B* **2000**, *62*, R7707−R7710.
(4) Ammar, A.; Cros, C.; Pouchard, M.; Jaussaud, N.; Bassat, J. M.; Villeneuve, G.; Duttine, M.; Ménétrier, M.; Reny, E. *Solid State Sci.* **2004**, *6*, 393−400.
(5) Karttunen, A. J.; Fassler, T. F.; Linnolahti, M.; Pakkanen, T. A. *Inorg. Chem.* **2011**, *50*, 1733−1742.
(6) Beekman, M.; Nolas, G. S. *J. Mater. Chem.* **2008**, *18*, 842−851.
(7) Jung, W.; Lörincz, J.; Ramlau, R.; Borrmann, H.; Prots, Y.; Haarmann, F.; Schnelle, W.; Burkhardt, U.; Baitinger, M.; Grin, Yu. *Angew. Chem.* **2007**, *119*, 6846−6850.
(8) Menke, H.; von Schnering, H. G. *Z. Anorg. Allg. Chem.* **1973**, *395*, 223−238.
(9) Nesper, R.; Curda, J.; von Schnering, H. G. *Angew. Chem.* **1986**, *98*, 369−370.
(10) Boehme, B.; Guloy, A. M..; Tang, Z.; Schnelle, W.; Burkhardt, U.; Baitinger, M.; Grin, Yu. *J. Am. Chem. Soc.* **2007**, *129*, 5348−5349.
(11) Ramachandran, K. G.; McMillan, P. F.; Dong, J.; Sankey, O. F. *J. Solid State Chem.* **2000**, *154*, 626−634.
(12) Bobev, S.; Sevov, S. C. *J. Am. Chem. Soc.* **1999**, *121*, 3795−3796.
(13) Zaikina, J. V.; Kovnir, K. A.; Haarmann, F.; Schnelle, W.; Burkhardt, U.; Borrmann, H.; Schwarz, U.; Grin, Yu.; Shevelkov, A. V. *Chem.—Eur. J.* **2008**, *14*, 5414−5422.
(14) Paschen, S.; Carrillo-Cabrera, W.; Bentien, A.; Tran, V. H.; Baenitz, M.; Grin, Yu.; Steglich, F. *Phys. Rev. B* **2001**, *64*, 214404.
(15) Carrillo-Cabrera, W.; Cardoso Gil, R.; Tran, V.-H.; Grin, Yu. *Z. Kristallogr.—NCS* **2002**, *217*, 181−182.
(16) Zhao, J. T.; Corbett, J. D. *Inorg. Chem.* **1994**, *33*, 5721−5726.
(17) Kirsanova, M. A.; Olenev, A. V.; Abakumov, A. M.; Bykov, M. A.; Shevelkov, A. V. *Angew. Chem., Int. Ed.* **2011**, *50*, 2371−2374.
(18) Sloan, E. D., Jr. *Clathrate hydrates of natural gases*, 2nd ed.; Marcel Dekker Inc.: New York, 1998.
(19) Cros, C.; Pouchard, M.; Hagenmuller, P. *Bull. Soc. Chim. Fr.* **1971**, 379−386.
(20) Kaltzoglou, A.; Ponou, S.; Fässler, T. F. *Eur. J. Inorg. Chem.* **2008**, 4507−4510.
(21) Saramat, A.; Svensson, G.; Palmqvist, A. E. C.; Stiewe, C.; Mueller, E.; Platzek, D.; Williams, S. G. K.; Rowe, D. M.; Bryan, J. D.; Stucky, G. D. *J. Appl. Phys.* **2006**, *99*, 023708.
(22) Nolas, G. S.; Cohn, J. L.; Slack, G. A.; Schjuman, S. B. *Appl. Phys. Lett.* **1998**, *73*, 178−180.
(23) Anno, H.; Hokazono, M.; Takakura, H.; Matsubara, K. *IEEE Proceedings of the 24th International Conference on Thermoelectrics (ICT 05)*, Clemson, SC, 2005; IEEE: New York, 2005; pp 102−105.
(24) Johnsen, S.; Thomsen, B.; Christensen, M.; Madsen, G. K. H.; Nygren, M.; Iversen, B. B. *IEEE Proceedings of the 26th International Conference on Thermoelectrics (ICT 07)* Jeju Island, South Korea, 2007; IEEE: New York, 2007; pp 219−222.
(25) Zeiringer, I.; Melnychenko-Koblyuk, N.; Grytsiv, A.; Bauer, E.; Giester, G.; Rogl, P. *J. Phase Equilib.* **2011**, *32*, 115−127.
(26) Zhang, H.; Borrmann, H.; Oeschler, N.; Candolfi, C.; Schnelle, W.; Schmidt, M.; Burkhardt, U.; Baitinger, M.; Zhao, J. T.; Grin, Yu. *Inorg. Chem.* **2011**, *50*, 1250−1257.
(27) Akselrud, L. G.; Zavalii, P. Yu.; Grin, Yu.; Pecharsky, V. K.; Baumgartner, B.; Wölfel, E. *Mater. Sci. Forum* **1993**, *133−136*, 335−340.
(28) Brandenburg, K. *Diamond 3.0*; Crystal Impact GbR: Bonn, Germany, 1997−2004.
(29) Jepsen, O.; Burkhardt, A.; Andersen, O. K. *The Program TB-LMTO-ASA*, version 4.7; Max-Planck-Institut für Festkörperforschung: Stuttgart, Germany, 1999.
(30) von Barth, U.; Hedin, L. *J. Phys. C* **1972**, *5*, 1629−1642.
(31) Andersen, O. K. *Phys. Rev. B* **1975**, *12*, 3060−3083.
(32) Koepernik, K.; Eschrig, H. *Phys. Rev. B* **1999**, *59*, 1743−1757.
(33) Kohout, M. *Int. J. Quantum Chem.* **2004**, *97*, 651−658.
(34) Kohout, M.; Wagner, F. R.; Grin, Yu. *Int. J. Quantum Chem.* **2006**, *106*, 1499−1507.
(35) Kohout, M. *Faraday Discuss.* **2007**, 43−54.
(36) Bader, R. F. W. *Atoms in Molecules, A Quantum Theory*; Clarendon Press and Oxford University Press Inc.: New York, 1994.
(37) Kohout, M. *DGrid*, 4.6, http://www.cpfs.mpg.de/~kohout/dgrid.html, 2011.
(38) Nguyen, L. T. K.; Aydemir, U.; Baitinger, M.; Bauer, E.; Borrmann, H.; Burkhardt, U.; Custers, J.; Haghighirad, A.; Hoefler, R.; Luther, K. D.; Ritter, F.; Assmus, W.; Grin, Yu.; Paschen, S. *Dalton Trans.* **2010**, *39*, 1071−1077.
(39) Cros, C.; Pouchard, M.; Hagenmuller, P. *J. Solid State Chem.* **1970**, *2*, 570−581.
(40) von Schnering, H. G.; Llanos, J.; Peters, K.; Baitinger, M.; Grin, Yu.; Nesper, R. *Z. Kristallogr.—NCS* **2011**, *226*, 9−10.
(41) Kovnir, K.; Stockert, U.; Budnyk, S.; Prots, Y.; Baitinger, M.; Paschen, S.; Shevelkov, A. V.; Grin, Yu. *Inorg. Chem.* **2011**, *50*, 10387−10396.
(42) Beekman, M.; Schnelle, W.; Borrmann, H.; Baitinger, M.; Grin, Yu.; Nolas, G. S. *Phys. Rev. Lett.* **2010**, *104*, 018301.
(43) Barron, T. H. K.; White, G. K. *Heat Capacity and Thermal Expansion at Low Temperatures*; Kluwer Academics/Plenum Publishers: New York, 1999; p 153ff.
(44) Emsley J. *Die Elemente*; Walter de Gruyter: Berlin-New York, 1994; pp 78−81.